# Photorefractive Fe:$LiNbO_3$ crystal thin plates for optical information processing

**Shiuan Huei Lin, Mei Li Hsieh, and Ken Yuh Hsu**

*Institute of Electro-Optical Engineering, National Chiao Tung University, Hsin-Chu, Taiwan*

**Tai Chiung Hsieh**

*Department of Electro-Physics, National Chiao Tung University, Hsin-Chu, Taiwan*

**Sheuan-Perng Lin, Tung-Sheng Yeh, Long-Jang Hu, Chin-Hwa Lin, and Hong Chang**

*Materials Research and Development Center, Chung Shan Institute of Science and Technology, Lung-Tan, Taiwan*

Received November 16, 1998; revised manuscript received March 22, 1999

The effects of the donor acceptor concentration ratio in iron-doped lithium niobate (Fe:$LiNbO_3$) crystal plates on photorefractive response time and on grating diffraction efficiency are studied both theoretically and experimentally. The results provide a useful guide for designing photorefractive plates for optical information-processing applications. Two devices for real-time image recognition have been demonstrated: a photorefractive joint-transform correlator and a VanderLugt correlator. The former emphasizes fast response time, and the latter emphasizes high diffraction efficiency. By appropriate adjustment of the dopant concentration and the ratio of the donor acceptor levels, photorefractive Fe:$LiNbO_3$ crystals that facilitate specific applications have been designed and fabricated. Shift-invariant image correlations have been achieved. © 1999 Optical Society of America [S0740-3224(99)01307-7]

*OCIS codes:* 190.5330, 200.3050, 160.3730, 160.5320, 100.4550, 100.5010.

## 1. INTRODUCTION

Recently photorefractive $LiNbO_3$ crystals have been studied for such optical information-processing applications as optical interconnections, optical neural networks, and volume holographic storage.[1–5] The advantages of this material are that high-optical-quality crystal with larger diameters can be grown and that the photorefractive characteristics of the crystal can be modified by addition of various dopant impurities, adjustment of the atmosphere for the thermal annealing process, or both. Typical photorefractive $LiNbO_3$ crystals are cut into thicknesses of a few millimeters to ~1 cm, and the dopant concentrations of the iron impurities are in the range 0.01–0.05 mol. %. These thicknesses and dopant concentrations provide suitable optical absorption for producing the photorefractive effect. At the same time they permit good transmission of optical information.[6–8] Under moderate illumination intensities (watts per square centimeter) the characteristic time for writing a hologram in a Fe:$LiNbO_3$ crystal is of the order of minutes, quite long compared with that of other photorefractive crystals such as $Bi_{12}SiO_{20}$ (milliseconds) and $BaTiO_3$ (a few seconds).[9,10] Staebler and co-workers demonstrated that transition-metal impurities, especially iron dopants, can enhance photorefractive sensitivity.[11–14] High sensitivities were also observed in heavily reduced samples of the lightly doped $LiNbO_3$ crystals.[15] However, in the range of visible light, iron dopants also increase the optical absorption coefficients of the crystals. As a result, obtaining enough transmission for the output detection required the dopant concentrations to be limited to a range of 0.01–0.05 mol. % for samples a few millimeters thick. The response-time constant for these samples was in the range of minutes. Based on Yeh's determination of the rate of photon absorption,[16] a theoretical limit for the response time of $LiNbO_3$ crystals can be estimated that is much faster. This suggests that changing the dopant concentrations provides one way to improve the response speed of $LiNbO_3$ and to adjust the photorefractivity of the material for the specific purpose of optical information processing.

In this paper we present a study of heavily iron-doped $LiNbO_3$ crystals. In particular, we focus on the effect of dopant concentration on the diffraction efficiency and the recording-time constant of the holographic grating. To alleviate the problem of large optical absorption in these heavily doped materials (0.06–1.5 mol. %), we use *x*-cut crystals polished into thin plates. This special arrangement makes the crystals useful for optical information applications that need thin dynamic holographic media. In what follows, theoretical analysis and optical experiments for thin Fe:$LiNbO_3$ plates are described. The results show that heavily doped impurities in Fe:$LiNbO_3$ crystals induce weak diffraction efficiency and a fast temporal response. They also show that the doping concentration in Fe:$LiNbO_3$ crystal can be adjusted such that the grating

0740-3224/99/071112-08$15.00 

diffraction and the temporal characteristics of the thin crystal can be tailored for particular image-processing applications. Two examples of optical image recognition with these crystal plates are experimentally demonstrated. In these two cases, two different methods of optimizing either the temporal response or the diffraction efficiency of the crystal plates are discussed.

## 2. CHARACTERISTICS OF THE THIN PHOTOREFRACTIVE CRYSTAL PLATES

It is well known that, in response to a distribution of light intensity, a refractive-index grating can be recorded in a photorefractive crystal. Based on the band transport model proposed by Kukhtarev[17] and Kukhtarev *et al.*,[18] this phenomenon can be explained as being due to three processes: photoexcitation, transport and retrapping of free carriers, and the linear electro-optic effect. When the crystal is illuminated by incident light, the photons are absorbed and photocarriers are generated from donor impurities. The photogenerated carriers are transported in the conduction band by diffusion and drift and recaptured by the ionized impurities; thus a space-charge field distribution is created. Finally, a refractive-index grating is induced in the crystal by the Pockels effect. Because the photocarriers are generated from and retrapped by the impurities and defects, the empty traps $N_A$ (acceptors) and the occupied traps $N_D$ (donors) are key parameters for determining the photorefractivity of the crystal. From Kogelnik's coupled-wave theory,[19] the intensity diffraction efficiency $\eta$ and the response-time constant $\tau$ of a transmission photorefractive grating can be derived as

$$\eta = \exp(-\alpha d)\sin^2\left(\frac{\pi d}{2\lambda\cos\theta} n^3 r_{\text{eff}} E_{\text{SC}}\right), \tag{1}$$

where

$$\alpha = s(N_D - N_D{}^i)h\nu, \tag{2}$$

$$E_{\text{SC}} = \text{Re}\left(\frac{iE_d - E_0}{1 + (E_d/E_q) + i(E_0/E_q)} \frac{I_1}{I_0}\right), \tag{3}$$

$$\tau = \frac{N_A}{sI_0N_D} \frac{E_d + E_\mu + iE_0}{E_d + E_q + iE_0}. \tag{4}$$

Equations (1)–(4) show that the diffraction efficiency and the time constant of the photorefractive gratings are complicated functions of donor and acceptor concentrations. From Eq. (1) it can be seen that there are two factors that affect diffraction efficiency: the exponentially decaying term, which is due to the material absorption, and the square of a sinusoidal term, which relates to the photorefractivity of the crystal and is an increasing function of the coupling constant (i.e., the argument of the sine function). Both the absorption coefficient and the coupling constant depend on the impurity concentration of the crystal. Equation (2) shows that the absorption coefficient increases linearly as the donor concentration increases. Thus the optical transmission of the crystal decreases exponentially as the dopant concentration increases. On the other hand, in Eq. (3) the coupling constant is intertwined with the material properties and the incident conditions of the recording beams.

From Eqs. (1)–(4) and the parameters given in Table 1 the diffraction efficiency can be calculated as a function of the donor concentration. The result is shown in Fig. 1, with the ratio $\xi = N_A/N_D$ as a parameter. It can be seen that, for a given $\xi$, the diffraction efficiency increases rapidly to its maximum value when the donor concentration is increased. A further increase in donor concentration causes strong optical absorption and results in a decrease of diffraction efficiency. The figure also shows that the maximum value of the diffraction efficiency increases as the ratio $\xi$ increases, whereas the location of the maximum occurs with a smaller donor concentration. This behavior is in agreement with other experimental results

**Table 1. Parameters for the Computer Simulations**

| Symbol | Meaning | Value |
|---|---|---|
| $\alpha$ | Optical absorption coefficient | |
| $E_{\text{SC}}$ | Space-charge field | |
| $E_d$ | Diffusion field | $K(k_BT/q)$ |
| $E_q$ | Saturation field | $qN_A/\langle\epsilon\rangle K$ |
| $E_\mu$ | Drift field | $\gamma N_A/\langle\mu\rangle K$ |
| $E_0$ | External applied field | Zero (in our case) |
| $N_D{}^i$ | Ionized donor impurity | |
| $h\nu$ | Photon energy | 2.42 eV |
| $k_B$ | Boltzmann Constant | $1.38 \times 10^{-23}$ J/K |
| $T$ | Temperature | 300 K |
| $q$ | Electron charge | $1.6 \times 10^{-19}$ C |
| $K$ | Grating vector | |
| $d$ | Thickness of the crystal | 36 $\mu$m |
| $2\theta$ | Angle between two writing beams | 4.7° |
| $I_1/I_0$ | Modulation depth | 0.01 |
| $\gamma$ | Electron-ionized trap recombination rate | $1 \times 10^{-9}$ cm$^3$/s |
| $\langle\mu\rangle$ | Effective electron mobility | 0.8 cm$^2$/V s |
| $s$ | Cross section for photoexcitation | 0.26 cm$^2$/J |
| $\lambda$ | Wavelength of input beam | 514.5 nm |
| $r_{\text{eff}}$ | Effective electro-optical coefficient | $31 \times 10^{-12}$ m/V |
| $\langle\epsilon\rangle$ | Effective dielectric constant | $32\epsilon_0$ |

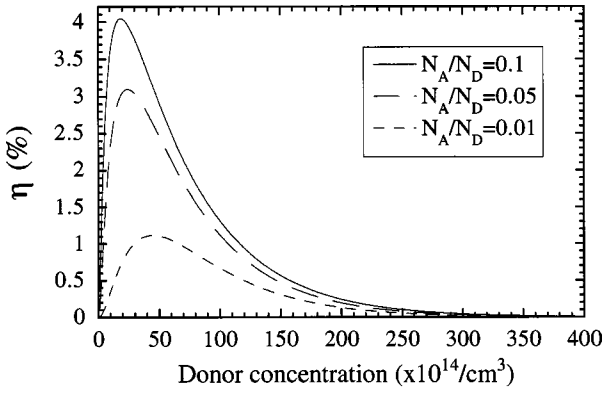


Fig. 1. Diffraction efficiency versus donor concentration for three ratios $N_A/N_D$ (theoretical analysis).

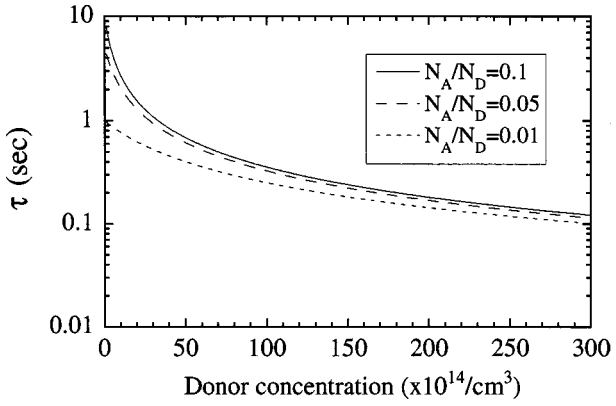


Fig. 2. Response-time constant versus donor concentration for three ratios $N_A/N_D$ (theoretical analysis).

in which the photorefractivity of a lightly doped Fe:$LiNbO_3$ crystal was significantly improved when the crystal was heavily reduced in an argon (or nitrogen) atmosphere.[14,15] To optimize diffraction efficiency, a trade-off between the absorption and the photorefractivity of the crystal should be made. This trade-off strongly depends on the thickness of the crystal plate.

It is also interesting to see how the dopant concentration affects the time constant for recording gratings in the photorefractive crystal. Equation (4) shows that the intrinsic photorefractive response time of the crystal is proportional to the ratio $\xi = N_A/N_D$. As the ratio increases, the intrinsic response time increases, which leads to an increase in the time constant of the crystal (i.e., the response speed decreases). By using Eq. (4) and the parameters given in Table 1 one can calculate the time constant for recording the photorefractive grating as a function of the dopant concentration for various ratios of $\xi$. The result is shown in Fig. 2. It can be seen that, in all cases for different ratios of $\xi$, the time constant decreases monotonically as the donor concentration increases. The slope becomes smoother as the ratio decreases. When the donor concentration is larger than $2 \times 10^{16}/\mathrm{cm}^3$, the time constant approaches the fundamental limit (~milliseconds) given by Yeh's calculation.[11] However, because of strong absorption, we need thin plates to provide enough light transmission.

In optical information-processing applications the diffraction efficiency and the response time of the photorefractive crystal are both important factors. The speed of formation of the gratings determines the time required for updating the dynamic memories, and the diffraction efficiency of the grating determines the signal-to-noise ratio of the output signal. Figures 1 and 2 provide a useful guide for designing the crystal plate.

In what follows, we consider two different applications. The first is a VanderLugt correlator. For this application, first the matched filter is recorded and then the images to be recognized are present in real time. The time constant is relevant only when the matched filter is being updated. On the other hand, a strong correlation peak can provide a large signal-to-noise ratio. Thus the diffraction efficiency is more important than the response time. For a given thickness of the crystal plate, in the large-$K$ regime ($K \gg k_D$) the donor concentration for maximizing the diffraction efficiency can be derived as

$$N_D = \frac{1}{d\sinh\nu C\xi(1-\xi)}\tan^{-1}(C\xi),$$
$$\approx \frac{1}{d\sinh\nu(1-\xi)}, \quad C\xi \ll 1, \tag{5}$$

where

$$C = \frac{e\pi n^3 I_1}{\lambda s I_0 \epsilon K h\nu\cos\theta} r_{\mathrm{eff}},$$

and the maximum diffraction efficiency is given by

$$\{\eta\}_{\max} = \frac{(C\xi)^2}{1+(C\xi)^2}\exp\left[-\frac{1}{C\xi}\tan^{-1}(C\xi)\right]$$
$$\propto (C\xi)^2, \quad C\xi \ll 1. \tag{6}$$

Expression (5) shows that the required concentration decreases as the ratio $\xi$ or the thickness of the crystal plate increases if $\xi \ll 1$. In contrast, relation (6) shows that the maximum diffraction efficiency increases as the ratio $\xi$ increases if $\xi \ll 1$. Therefore a lightly doped crystal is good for the VanderLugt correlator application. We can enhance the diffraction efficiency by increasing the ratio $\xi$ of the crystal by a reduction reaction in the annealing process.

The second application is a joint-transform correlator. For this application the spatial filters are updated in real time. Thus the writing speed of the grating is as important as the diffraction efficiency. If the required minimum diffraction efficiency is given, then the required donor concentration can be derived. For weak diffraction efficiency (coupling constant $\ll 1$), the donor concentration is a solution of a transcendental equation given by

$$\left[\frac{N_D}{1+C_2\xi(1-\xi)N_D}\right]^2$$
$$\times \exp[-\kappa(1-\xi)N_D] = \eta_{\min}\left[\frac{1}{C_1\xi(1-\xi)}\right]^2, \tag{7}$$

where

$$\kappa = s d h\nu,$$
$$C_1 = \frac{e\pi d I_1}{2 I_0 \lambda\langle\epsilon\rangle K\cos\theta} n^3 r_{\mathrm{eff}},$$
$$C_2 = \frac{e^2}{\langle\epsilon\rangle k_B T K}.$$

The maximum updating speed of the reference image can be obtained by substitution of the solution of the transcendental equation into Eq. (4). Note that in Eq. (4) the time constant increases as the ratio $N_A/N_D$ increases. To obtain a thin plate with fast response, it is necessary to keep the ratio $N_A/N_D$ as small as possible. This will reduce the diffraction efficiency of the plate. Thus one should compromise between these two requirements by using the plots of Figs. 1 and 2.

Now we describe the experimental measurements of our thin crystal plates. To prepare a series of the crystal plates, we grew $LiNbO_3$ single crystals with $Fe_2O_3$ doping

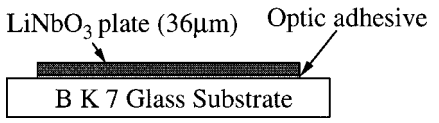


Fig. 3. Structure of the thin crystal plate.

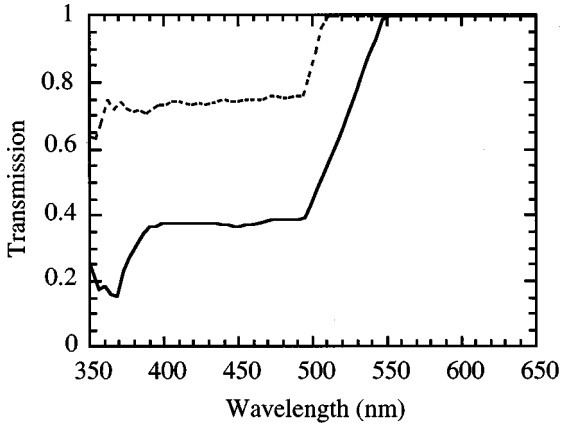


Fig. 4. Transmission spectra of the 0.06-mol. % (dashed curve) and the 1.5-mol. % (solid curve) iron-doping $LiNbO_3$ plates.

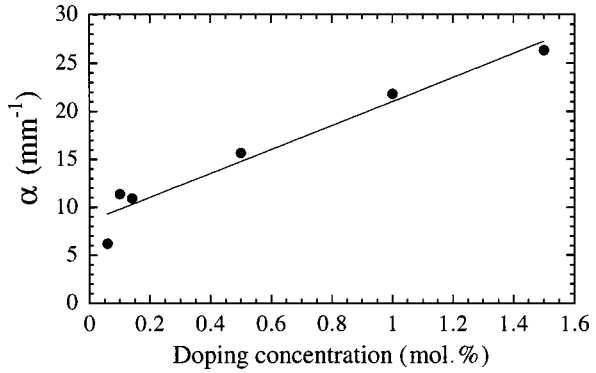


Fig. 5. Experimental measurement of the absorption coefficients of the crystal plates versus the iron-doping concentrations.

concentrations that varied from 0.06 to 1.5 mol. % by the Czochraski technique. The crystals were cut into thin *x* plates and then attached to an optical glass (BK 7) substrate. Finally they were polished to a thickness of ~36 $\mu$m. The structure of the thin plate is shown in Fig. 3. First we measured the transmission spectrum of these plates in the spectral range 350–650 nm. Typical transmission spectra of the 0.06- and 1.5-mol. % plates are shown in Fig. 4. Also, the absorption coefficient at 514.5 nm is measured as a function of the dopant concentration, as shown in Fig. 5. It can be seen that the absorption coefficient is almost a linear function of the dopant concentration, in agreement with our theoretical analysis derived in Eq. (2). Note that an intrinsic absorption coefficient exists in undoped crystal that might be a result of crystal defects or impurities during crystal growth.

To measure the photorefractivity of different plates we constructed a typical four-wave mixing system (as shown in the inset of Fig. 6). Two extraordinarily polarized plane waves from an argon laser (with a wavelength of 514.5 nm) were incident symmetrically into the crystal plate such that the grating vector was parallel to the *c* axis. The intersection angle between the writing beams was 4.7°. The total intensity of the writing beam was 1 $W/cm^2$. An extraordinary plane wave from the same laser (with an intensity of ~83 $mW/cm^2$) was incident from the opposite side of the plate to monitor the temporal behavior of the first-order diffraction. As much as 3 orders of diffraction was observed. Figure 6 shows a typical curve of the temporal response of grating formation and decay for a crystal plate with a dopant concentration of 1.0 mol. %. It is estimated that the buildup time constant (which is defined as the slope of growth of the grating amplitude obtained from the square root of the diffracted power) of the grating is ~28 ms and that the decay time is ~7.8 ms. By comparing these time constants with those of the conventional lightly doped Fe:$LiNbO_3$ crystals (which have a long time constant of dark storage and a slow temporal response in the range of minutes to hours), we see that heavy iron doping significantly improves the response speed of the crystal plate.

The relationship between the time constant for grating buildup and the dopant concentrations was measured and is shown in Fig. 7. The figure shows that the response time decreases with increasing dopant concentration. As the dopant concentration is increased to 1.5 mol. %, the time constant decreases to 12.5 ms. This value is close to the fundamental limit calculated from Yeh's model. Inasmuch as our crystals were grown without any special annealing processing, the exact values of the ratio $\xi$ of

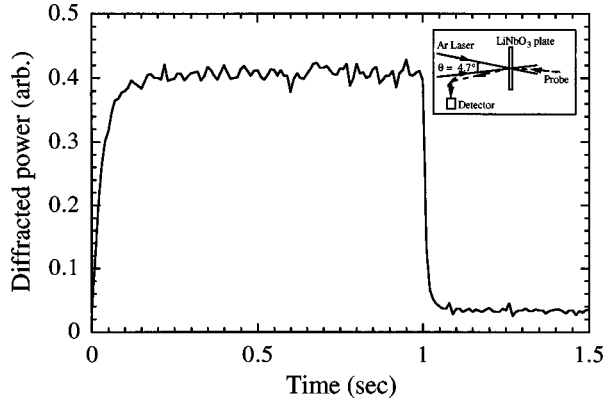


Fig. 6. Typical temporal behavior of grating formation and decay for the 1.0-mol. % iron-doped $LiNbO_3$ plate.

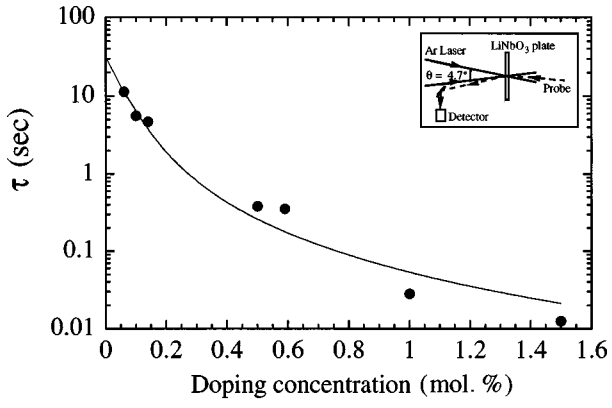


Fig. 7. Experimental measurement of the buildup time constant for grating formation versus the iron-doping concentrations for the crystal plates.

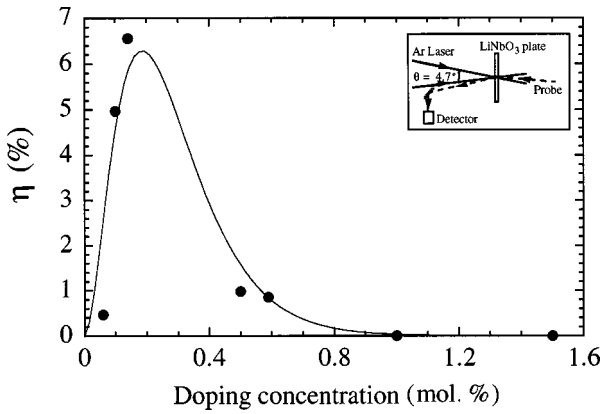


Fig. 8. Experimental measurement of diffraction efficiency versus the iron-doping concentrations for the crystal plates.

these plates were unknown. However, the experimental curve still shows a trend similar to that of the theoretical prediction. We also measured the diffraction efficiency as a function of the dopant concentration. The results are shown in Fig. 8. It can be seen that the diffraction efficiency increases rapidly as the dopant concentration increases, reaching a maximum near a concentration of 0.14 mol. %, and then decreases because of strong optical absorption. This trend is again in coincidence with our theoretical prediction.

Under our experimental conditions the time constant for the crystal plate with the maximum diffraction efficiency (i.e., the crystal plate with 0.14-mol. % iron-doping concentration) is 4.7 s. This rate is slow and is not suitable for dynamic grating applications such as a joint transform correlator. Thus a trade-off between diffraction efficiency and response speed has to be considered when we design a photorefractive crystal for optical processing applications. In what follows, we describe two optical correlators that utilize $LiNbO_3$ crystal plates.

## 3. REAL-TIME OPTICAL INFORMATION-PROCESSING APPLICATIONS

### A. Joint-Transform Correlator

Figure 9 is a generic diagram of a photorefractive joint-transform correlator (PRJTC). Two input patterns, $u_1$ and $u_2$, are Fourier transformed and interfered to write a refractive-index grating in the crystal plate. This index grating is read out by a plane wave, which is incident from the back side of the crystal plate. For the PRJTC we operated the thin plate in the Raman–Nath regime. To achieve this operation, we designed the intersection angle between the writing beams and the thickness of the crystal plate such that the hologram parameter $Q < 1$. Thus the $m$th-order diffraction from the photorefractive grating is proportional to the $m$th-order Bessel function[20]:

$$E_{dm} = U_3 J_m\left(\frac{2\pi}{\lambda\cos\theta_R} n_1 d\right), \quad m = \pm 1, \pm 2, \pm 3, \ldots, \tag{8}$$

where $U_3$ is the amplitude of the reading beam, $\theta_R$ is the incident angle of the reading beam, and $n_1$ is the refractive-index perturbation induced by the interference pattern of the writing beams in the photorefractive crystal plate. Based on the photorefractive theory, $n_1$ is given by

$$n_1 \sim U_1^* U_2 + U_1 U_2^*, \tag{9}$$

where $U_1$ and $U_2$ are the amplitudes of two writing beams in the crystal plate, which are Fourier transforms of input images $u_1$ and $u_2$, and $*$ represents complex conjugation. Under the condition that the arguments of the Bessel functions are much smaller than 1, the first-order diffraction can be approximated as

$$E_{d1} = U_3 J_1\left(\frac{2\pi}{\lambda\cos\theta_R} n_1 d\right)$$

$$\approx U_3 \frac{2\pi}{\lambda\cos\theta_R} n_1 d$$

$$\propto U_3(U_1^* U_2 + U_1 U_2^*). \tag{10}$$

If the $U_3$ is a plane wave (i.e., $u_3$ is a point source), relation (10) represents a spatial filter. The Fourier transform of the +1-order diffraction gives the output

$$C(x', y') = u_1(x, y) \otimes u_2(x, y), \tag{11}$$

where $\otimes$ represents the correlation operation. The above analysis shows that a PRJTC system can be achieved by use of a thin photorefractive crystal plate in the Raman–Nath diffraction regime (i.e., $Q < 1$). There are several advantages to this operation. First, the planar grating characteristics of the Raman–Nath diffraction make this system shift invariant. Thus the correlation signal will not be degraded when either the reference or the target image is shifted in the input plane. Second, there is no requirement for Bragg matching of the reading beam, which can be incident into the planar hologram from an

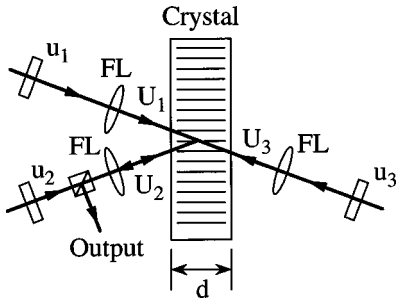


Fig. 9. Generic diagram of a photorefractive correlator: FL's, Fourier lens; other abbreviations defined in text.

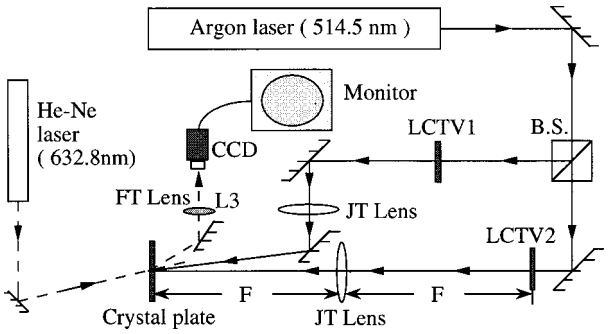


Fig. 10. Schematic diagram of the PRJTC: FT, Fourier transform; JT, joint transform; B.S., beam splitter; other abbreviations defined in text.

arbitrary angle. If the response speed of the crystal plate is fast enough, both the reference and the input images can be updated in real time.

A schematic diagram of our PRJTC system is shown as Fig. 10. A collimated extraordinarily polarized beam from an argon laser with a wavelength of 514.5 nm and a total intensity of 1 W/cm$^2$ was split into two beams. Each beam passed through a liquid crystal television (LCTV) that carried the input images. LCTV1 showed the reference object, and LCTV2 showed the target object. These two images were Fourier transformed and intersected in the crystal. The interference pattern induced a refractive-index grating in a Fe:$LiNbO_3$ crystal plate. The focal length of the Fourier lens was 40 cm, and the width of the LCTV was 3 cm. Therefore the minimum intersection angle should be larger than 4.5°, such that two LCTV's can be separated. Under this condition, achieving a Raman–Nath regime ($Q < 1$) requires that the crystal plate be thinner than 36 $\mu$m. The correlation signal was read out by a plane wave from a He–Ne laser at a wavelength of 632.8 nm with an intensity of 82 mW/cm$^2$. Because the background scattering noise of the crystal plate observed in our experiments was ~82 $\mu$W/cm$^2$, the minimum required diffraction efficiency had to be larger than $1 \times 10^{-2}$, such that the correlation signals could be detected well. From Eq. (7), the concentration of the donors had to be smaller than $1 \times 10^{16}$/cm$^3$. At this doping level the response time of the crystal plate was ~250 ms. Therefore the updating rate of the target object, the reference objects, or both is limited to approximately four frames per second. In our experiments we picked up the crystal plate with a 0.59-mol. % iron-doping concentration. The plate's response time is ~352 ms.

Figures 11(a) and 11(b) are photographs of the experimental results. Figure 11(a) shows the input images to the PRJTC. At the left is the input image, which consists of three rows of Chinese words. At the right is the reference image, which is a Chinese character. Figure 11(b) shows the correlation output. The two correlation peaks demonstrate the shift-invariant property of this PRJTC system. In addition, if the reference object was updated at the rate of 1 frame/s, the correlation output followed the change at the same speed. The result is shown in Fig. 11(c), in which the upper trace represents the sequence of the input image that is generated by chopping of the input beam with an electronic shutter and the lower trace is the correlation peak detected by a photodetector. It can be seen that the system is capable of dynamic filter updating.

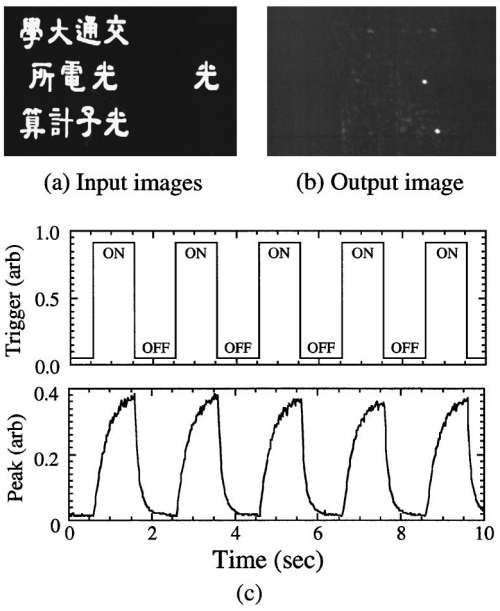


Fig. 11. (a), (b) Input images and correlation output for our PRJTC. (c) Temporal response of updating the reference image in the PRJTC.

### B. VanderLugt Correlator

Figure 9 can also be used as a generic diagram of a photorefractive VanderLugt correlator (PRVLC). In this case, $u_2$ is a point source and $u_1$ is the object wave. Thus $U_2$ is a plane wave and $U_1$ is the Fourier-transform spectrum of $u_1$. $U_1$ and $U_2$ interfere to record a holographic matched filter in the crystal plate. PRVLC operation needs a 4-$F$ optical system, where $F$ is a focal length. To reduce the space of the optical system we chose a focal length of 10 cm for the Fourier-transform lens in our experiments. Because the width of our LCTV is 3 cm, separating the input image from the reference requires that the intersection angle between the plane wave and the center of the reference image be at least 8.55°. Thus, $Q > 1$, the 36 $\mu$m crystal plate could not be operated in the Raman–Nath regime, and the system should be analyzed by use of the coupled-wave theory of the thick hologram. According to Kogelnik's analysis for a transmission volume phase grating, the diffracted amplitude is given by[19]

$$E_d = -iU_3 \exp\left(-\frac{\alpha d}{2} + i\frac{\Delta\beta}{2}d\right) \times \frac{n_1\pi/\lambda\cos\theta_R}{[r^2 + (\Delta\beta/2)^2]^{1/2}} \sin\left\{rd\left[1 + \left(\frac{\Delta\beta}{2r}\right)^2\right]^{1/2}\right\}, \quad (12)$$

with

$$r = \frac{\pi}{\lambda\cos\theta_R} n_1,$$

$$\Delta\beta = -\frac{4n\pi}{\lambda}\sin\theta\Delta\theta - \frac{4n\pi}{\lambda^2}\frac{\sin^2\theta}{\cos\theta}\Delta\lambda,$$

where $U_3$ is the amplitude of the reading beam, $\Delta\beta$ is a dephasing term that is due to the Bragg mismatch of the reading beam, $\theta$ is the Bragg angle, $\theta_R$ is the incident angle of the reading beam, and $n_1$ is the refractive-index perturbation induced by the interference pattern of the writing beams in the photorefractive crystal plate. The Bragg mismatch comes from a small-angle deviation $\Delta\theta$, which is induced by a small shift of the target object in the $u_3$ plane, and a wavelength deviation $\Delta\lambda$, which is induced by a reading beam with a different wavelength. Note that the dephasing factor $\Delta\beta$ could be eliminated if the reading beam were incident at the Bragg angle for the different wavelength. Taking $u_3$ as the complex conjugation and with 180° rotation of the target object, the Fourier transform of the diffracted wave can be derived to be

$$C(x', y') \propto u_1(x, y) \otimes u_3(x, y)\mathrm{sinc}\{rd[1 + (\Delta\beta/2r)^2]^{1/2}\}. \tag{13}$$

Relation (13) shows that image correlation can be achieved by use of the PRVLC structure. Note that the sinc function serves as a window function if the incident angle of $U_3$ does not match the Bragg condition. In other words, the correlation peak degrades when the target object is shifted in the $u_3$ plane. The sinc function thus serves as a limit on the viewing range of the target object. If the range of shift invariance is defined as a shift in the target object such that the autocorrelation peak decays to the first zero of the sinc function, then the range $\Delta$ can be derived as

$$\Delta = \frac{f\lambda r}{\pi \sin\theta}\left[\left(\frac{\pi}{rd}\right)^2 - 1\right]^{1/2}, \tag{14}$$

where $f$ is the focal length of the Fourier-transform lens. Note that this range is inversely proportional to the thickness of the crystal plate when $rd \ll \pi$. Thus, the thinner the crystal plate, the larger the range for shift invariance. However, as the thickness of the crystal plate decreases, the diffraction efficiency of the photorefractive grating also decreases. Of course, as shown in Eq. (14), one can increase the shift-invariant range by increasing the focal length of the lens. However, doing so will cause the system to occupy a larger space. Hence, to maintain rigid space and also obtain a large shift-invariant range of the system for a given crystal thickness it is necessary to optimize the diffraction efficiency by proper adjustment of the dopant concentration.

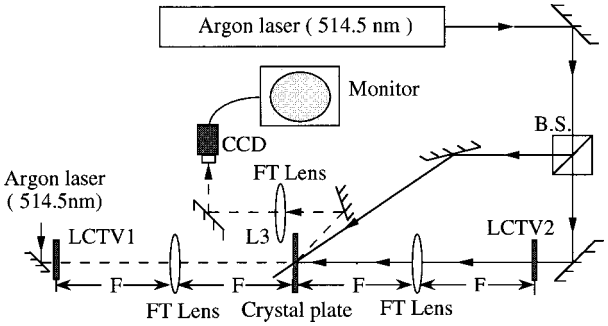


Fig. 12. Schematic diagram of our four-wave-mixing PRVLC. FT, Fourier transform; B.S., beam splitter; other abbreviations defined in text.

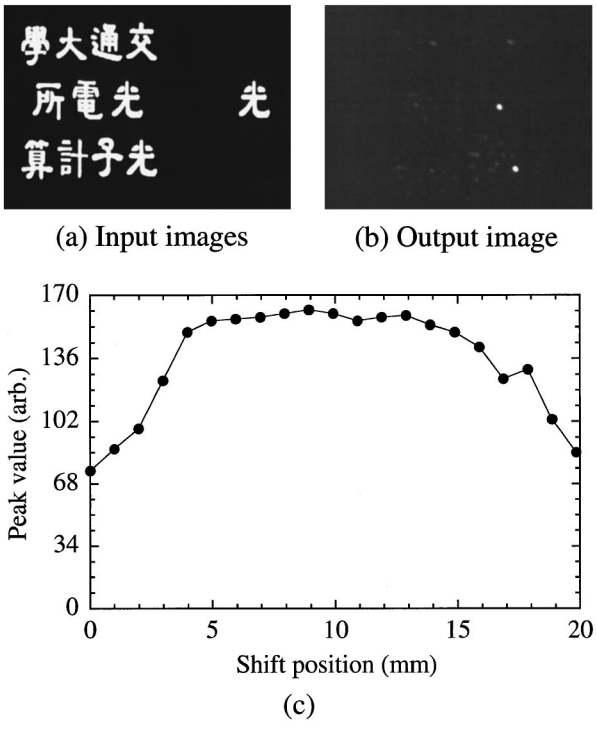


Fig. 13. (a), (b) Input images and correlation output for our PRVLC. (c) Correlation peak versus shift-invariant distance for our PRVLC.

A schematic diagram of our PRVLC system is shown in Fig. 12. A collimated extraordinarily polarized beam from an argon laser at a wavelength of 514.5 nm with a total intensity of 1 W/cm$^2$ was split into two beams: The beam that passed through LCTV1 was used for carrying the reference images, and the other beam was used as the reference wave. The two beams interfered at an intersection angle of 10° upon the Fe:$LiNbO_3$ crystal plate, and the matched filter was recorded. The matched filter was read out by the target objects shown on LCTV2, which was illuminated by the same laser with an intensity of 100 mW/cm$^2$. The correlation output was detected by a CCD camera in the Fourier plane of lens L3. The focal length of all the Fourier lenses was 10 cm, the screen size of the LCTV was 3 cm, and the thickness of the crystal plate was 36 $\mu$m. As we explained for the PRJTC, to overcome the scattering noise of the crystal plate the minimum diffraction efficiency of the grating must be larger than $4 \times 10^{-2}$. From expression (5), the concentration of the donors should be close to $2 \times 10^{14}$/cm$^3$. Using these parameters, we estimated the response time of the crystal plate to be ~2 s. Therefore the maximum updating rate of the matched filter was approximately one reference object in every 2 s. In our experiments we used a crystal plate with a 0.15-mol. % iron-doping concentration. The response time of our plate was ~4 s.

Figures 13(a) and 13(b) are photographs of the experimental results. Figure 13(a) shows the input images to the PRVLC. At the left is the input image and at the right is the reference image. Figure 13(b) shows the correlation output. The two correlation peaks demonstrate the shift-invariant property of this PRVLC system. In addition, if the target object is shifted in the $u_3$ plane, the correlation peak follows. The value of the correlation peak as a function of the shifted distance is shown in Fig. 13(c). The system is thus capable of shift-invariant correlation.

## 4. CONCLUSION

We have performed both a theoretical analysis and experimental studies of photorefractive characteristics by adjusting the donor acceptor concentration ratio in iron-doped lithium niobate (Fe:$LiNbO_3$) crystal plates. Our results show that the impurity doping concentration affects the grating diffraction efficiency and the temporal characteristics of the thin crystal plates. They provide a useful guide for designing photorefractive crystals for various optical information-processing applications. We have experimentally demonstrated two examples of real-

time optical image recognition by considering two different methods of optimization. In the PRJTC system, the fast response speed is necessary for achieving image recognition with the capability of dynamic filter updating. Thus a fast response is emphasized. According to our analysis, the time constant and the diffraction efficiency of the crystals both decrease when donor concentrations are at high dopant levels. Hence the speed of operation is limited by the detectable diffraction efficiency of the output signal under the scattering noise. The updating speed in our system is ~4 frames/s. On the other hand, in the PRVLC system, high diffraction efficiency is more important for achieving a compact correlator system with a large shift-invariant range. Thus the crystal plate is optimized to yield maximum diffraction efficiency. According to our analysis, the decrease in diffraction efficiency results mainly from optical absorption. Hence a lightly doped crystal is good for VanderLugt correlator application. One can enhance the diffraction efficiency by increasing the ratio $N_A/N_D$ through a crystal reducing process. Our analysis for $LiNbO_3$ crystal is valid in general; thus the results can be applied to other photorefractive crystals.

## ACKNOWLEDGMENT

Support for this research by the National Science Council of the Republic of China under contract NSC88-2215-E009-008 is gratefully acknowledged.

## REFERENCES

1. D. Psaltis, D. Brady, and K. Wagner, "Adaptive optical networks using photorefractive crystals," Appl. Opt. **27**, 1752–1759 (1988).
2. F. H. Mok, "Angle-multiplexed storage of 5000 holograms in lithium niobate," Opt. Lett. **18**, 915–917 (1993).
3. K. Y. Hsu, S. H. Lin, and T. C. Hsieh, "Photorefractive memories for real-time image processing," Opt. Mem. Neural Netw. **4**, 277–285 (1995).
4. K. Itoh, O. Matoba, and Y. Ichioka, "ODINN in LiN: optical dynamic interconnections for neural networks in lithium niobate," in *Photorefractive Fiber and Crystal Devices: Materials, Optical Properties, and Applications*, F. T. Yu, ed., Proc. SPIE **2529**, 71–81 (1995).
5. C. Sun, R. Tsou, J. Chang, and M. Chang, "Real-time photorefractive interferometer for dynamic phase perturbation by self-interference in $LiNbO_3$," Appl. Opt. **36**, 3581–3585 (1997).
6. H. Kurz, "Lithium niobate as a material for holographic information storage," Philips Tech. Rev. **37**(5/6), 109–120 (1977).
7. H. Vormann, G. Weber, S. Kapphan, and E. Kratzig, "Hydrogen as origin of thermal fixing in $LiNbO_3$:Fe," Solid State Commun. **40**, 543–545 (1981).
8. S. Yin, F. Zhao, H. Zhou, M. Wen, J. Zhang, and F. T. S. Yu, "Wavelength-multiplexed holographic construction using a Ce:Fe:$LiNbO_3$ crystal with a tunable visible-light diode laser," Opt. Commun. **101**, 317–321 (1993).
9. M. Peltier and F. Micheron, "Volume hologram recording and charge transfer process in $Bi_{12}SiO_{20}$ and $Bi_{12}GeO_{20}$," J. Appl. Phys. **48**, 3683–3690 (1977).
10. Y. Fainman, E. Klancnik, and S. H. Lee, "Optimal coherent image amplification by two-wave coupling in photorefractive $BaTiO_3$," Opt. Eng. (Bellingham) **25**, 228–234 (1986).
11. J. J. Amodei, W. Philips, and D. S. Staebler, "Improved electro-optic materials and fixing techniques for holographic recording," Appl. Opt. **11**, 390–396 (1972).
12. D. L. Staebler, W. Burke, W. Philips, and J. J. Amodei, "Multiple storage and erasure of fixing holograms in Fe-doped $LiNbO_3$," Appl. Phys. Lett. **26**, 182–184 (1975).
13. W. Phillips, J. J. Amodei, and D. S. Staebler, "Optical and holographic storage properties of transition metal doped lithium niobate," RCA Rev. **33**, 95–109 (1972).
14. P. Gunter and J. P. Huignard, *Photorefractive Materials and Their Applications* (Springer-Verlag, New York, 1988), Chap. 6.
15. R. Orlowski and E. Kratzig, "Holographic method for the determination of photo-induced electron and hole transport in electro-optic crystal," Solid State Commun. **27**, 1351–1354 (1978).
16. P. Yeh, "Fundamental limit of the speed of the photorefractive effect and its impact on device applications and material research," Appl. Opt. **26**, 602–605 (1987).
17. N. V. Kukhtarev, "Kinetics of hologram recording and erasure in electro-optic crystal," Sov. Tech. Phys. Lett. **2**, 438–440 (1976).
18. N. V. Kukhtarev, V. B. Markov, S. G. Odulov, M. S. Soskin, and V. L. Vinetskii, "Holographic storage in electro-optic crystals. I. Steady state," Ferroelectrics **22**, 949–960 (1979).
19. H. Kogelnik, "Coupled wave theory for thick hologram gratings," Bell Syst. Tech. J. **48**, 2909–2947 (1969).
20. For example, see P. Yeh, *Introduction to Photorefractive Nonlinear Optics* (Wiley, New York, 1993), Chap. 2.